

A FUSE Survey of the Rotation Rates of Very Massive Stars in the Small and Large Magellanic Clouds

Laura R. Penny

*Department of Physics and Astronomy
The College of Charleston
Charleston, SC 29424
pennyl@cofc.edu*

Douglas R. Gies

*Center for High Angular Resolution Astronomy and
Department of Physics and Astronomy,
Georgia State University, P. O. Box 4106, Atlanta, GA 30302-4106
gies@chara.gsu.edu*

ABSTRACT

We present projected rotational velocity values for 97 Galactic, 55 SMC, and 106 LMC O-B type stars from archival FUSE observations. The evolved and unevolved samples from each environment are compared through the Kolmogorov-Smirnov test to determine if the distribution of equatorial rotational velocities is metallicity dependent for these massive objects. Stellar interior models predict that massive stars with SMC metallicity will have significantly reduced angular momentum loss on the main sequence compared to their Galactic counterparts. Our results find some support for this prediction but also show that even at Galactic metallicity, evolved and unevolved massive stars have fairly similar fractions of stars with large $V \sin i$ values. Macroturbulent broadening that is present in the spectral features of Galactic evolved massive stars is lower in the LMC and SMC samples. This suggests the processes that lead to macroturbulence are dependent upon metallicity.

Subject headings: Stars: spectroscopic — stars: early-type — stars: rotation — Magellanic Clouds — ultraviolet: stars

1. Introduction

Stellar interior models are the backbone of modern stellar astrophysics. Their predictions are used in a myriad of applications including determinations of stellar masses from

observed luminosities and temperatures, studies of star clusters, population synthesis, stellar nucleosynthesis, chemical evolution, etc. Many factors are included in these extremely complex interior codes: overshooting, mass loss rates, opacities, convection. The latest addition to these models has been the inclusion of rotation and its subsequent effects on interior mixing (Meynet & Maeder 2000; Heger & Langer 2000; ?). With each additional advance in these codes, observers have been tasked with testing the new models by finding observable diagnostics. What do the new models predict that can be observed to either agree or disagree with the model? For massive stars the newest models are very interesting. Rotation induces interior mixing that changes the luminosities, lifetimes, effective temperatures, and surface abundances of these massive stars. The combined effect of mass loss and angular momentum in the models results in angular momentum loss; as the mass comes off it takes with it any angular momentum it may have had. This results in an evolution of surface rotation speed that varies depending upon the amount of mass loss.

The most striking prediction of the new models is the effect of rotation on the internal structure and subsequent luminosity and main sequence lifetime of the star. The models with rotation predict evolutionary tracks that become more luminous. This results from two effects: rotational mixing of H-fuel into the convective core and transport of He and other H-burning by-products into the radiative envelope. The first effect increases the mass of the convective core, while the second lowers the opacity of the envelope. Heger & Langer (2000) state, “As a result of these dependencies of the stellar evolutionary tracks in the HR diagram on the initial rotation rate, a given point in the HR diagram is not uniquely related to a single initial mass, even for core hydrogen burning stars.” This introduces a serious scatter in the mass-luminosity relation. In order to determine the evolutionary mass for an object, the luminosity, effective temperature, and the initial equatorial velocity of the star are needed, but this last parameter is indeterminable. One can attempt to test this prediction of rotationally induced overluminosity. To test if a single star is overluminous for its mass, first requires knowledge of the mass of the star. The only direct means to determine the mass is from binary systems. There are cases where members of a binary system with large equatorial velocities do appear overluminous for their masses (Penny, Gies, & Bagnuolo 1999). However other effects can also cause binary stars to appear overluminous, mass transfer being the most common. Also members of a binary pair exchange spin and orbital angular momentum as they evolve due to tidal interactions, making them poor tests of single star models.

The models also predict how the surface rotation rates should change as the stars evolve. For solar metallicity stars ($Z_{MW} = 0.020$) the most massive should slow their rotation drastically while still on the main sequence (MS). There are two competing factors that govern the surface rotation rates: (1) transfer of angular momentum from the inner parts to

the outer ones through meridional circulation and (2) angular momentum loss at the surface of the star through mass loss. The first of these is present in all rotating stars and is primarily dependent upon the rotation rate: the faster the spin, the more mixing occurs. The mass loss is from large stellar winds that are driven by line opacities associated with metallic elements. For stars at lower metallicities (i.e., Small Magellanic Cloud, $Z_{SMC} = 0.004$ and Large Magellanic Cloud, $Z_{LMC} = 0.007$), there are significantly lower numbers of metal atoms and therefore lower line opacity. Mass loss rates are lower and subsequent angular momentum loss rates are lower too. The rotation rates of massive stars at lower Z are predicted to remain almost constant during the MS. For example Figure 10 of Meynet & Maeder (2000) shows the evolution of surface rotational velocities as a function of time for a $20 M_{\odot}$ star at solar and SMC metallicity with an initial rotation speed of 300 km s^{-1} . By the late main sequence the rotation rate of the Galactic star has decreased to 140 km s^{-1} , while its SMC counterpart still has a rotation rate of 220 km s^{-1} .

It is interesting to consider what spectral class stars these models refer to, as stars do not come labeled with their initial masses. The new models predict that stars with initial masses smaller than $15 M_{\odot}$ do not slow significantly while on the MS even in the Milky Way. There is no metallicity dependence on their rotational evolution, i.e., a $12 M_{\odot}$ star at both solar and SMC metallicity have similar behavior. Our prime targets for testing purposes should be stars that started with 15 or more solar masses. In addition we see that after the end of the MS, the surface rotational velocities of even these massive stars drop precipitously in all metallicity environments. A star with an initial mass larger than $15 M_{\odot}$ spends its MS life as an O-type star (see Fig. 1). In fact, we see that despite expectations that luminosity classes of giant or supergiant describe post-MS stars, this is not possible for O spectral types. All O-type stars, regardless of their luminosity class, are core-hydrogen burning objects. They will eventually become B and A supergiants, but when they do they will have greatly increased radii, and decreased surface rotational velocities. They also do not exclusively populate these types. In Figure 1 we over plot the effective temperature line of 14900K , which corresponds to the luminosity class B3 I (Bohm-Vitense 1981). Even a star with initial mass of $7 M_{\odot}$ becomes a B3 I (according to Schaller et al. 1992, $T_{\text{eff}} = 15100\text{K}$, $\log g = 3.25$ occurs at age $= 4.32 \times 10^7$ yrs for the $7 M_{\odot}$ track). Early B-type supergiants are not an exclusive group and for stars with $M_{\text{ini}} \geq 15 M_{\odot}$, they represent stars past the end of the MS. As such they are not optimal targets for testing the predictions from the new stellar interior models.

There exists observational evidence that the predictions for solar metallicity stars are correct. Galactic O-type stars do slow down as they evolve along the main sequence (Conti & Ebbets 1977; Penny 1996; Howarth et al. 1997). There are few broad-lined stars among the more massive and more evolved objects. The fastest rotators are found among

the lower mass O stars. This agrees well with predictions: that the rotation rates should decrease while still on the MS; that the larger the initial mass, the faster the decrease in rotation; and that the more evolved MS stars should show the biggest decrease in rotation. Observationally only $V \sin i$ (projected rotational velocity) is determined in these studies due to the orientation of the polar axis to the line of sight (i). But with a large enough sample we can assume a random distribution of this inclination angle. While it is possible that some massive and evolved objects are observed pole-on, with a large sample it is unlikely that orientation effects can explain the observed trends.

Indirect support that massive stars at low metallicity do NOT slow down comes from a study by Maeder et al. (1999) who found a significant increase in the number ratio of Be/(B+Be) for decreasing metallicities in Galactic and MC clusters. They argue that the Be phenomenon is closely linked to rapid rotation, and so if the massive stars with low Z do not slow down, perhaps they produce more Be stars. We should note here that a Be star is a non-supergiant B-type star that has a significantly lower initial mass than the O-type objects. The models produced for low Z massive stars do not predict that stars with initial masses relating to Be-type will have metallicity dependent decrease in rotation rates while on the MS. However the initial velocities of these stars may vary with Z . The initial rotation rates of massive stars at low Z are not known. Maeder & Meynet (2001) have assumed that the initial rates are the same in the MC and Galaxy (since observational data are lacking). But the star formation process itself may be altered at smaller metallicity. Although no numerical models of the formation of massive stars at low Z have been produced, there are some possible origins of higher initial rotational velocities. A lower Z environment would have lower dust content and fewer metallic ions present in star forming regions so that the magnetic field of the contracting central mass is less coupled to the surrounding region. Also the lifetime of the accretion disk is likely related to its opacity, which will decrease with lower metallicity. These factors would result in less angular momentum loss during star formation, leading to higher initial rotational velocities.

There are few direct measurements of the rotation rates of massive stars at low metallicities. Maeder et al. (1999) state “Of course, direct observations of $V \sin i$ in LMC and SMC clusters are very much needed in order to substantiate the above results.” Only a few studies have been published to date on the rotation rates of massive stars at low metallicity. Some have focused on early B type stars (Keller 2001; Dufton et al. 2006), but again we caution that these cooler objects are not exclusively produced by stars with 15 or more solar masses and are often significantly larger than their terminal age main sequence (TAMS) radii.

We made a study of 44 O-type stars in the SMC and LMC utilizing archival HST observations (Penny et al. 2004). We compared the cumulative distribution function (CDF)

of the $V \sin i$ values for Galactic, LMC and SMC evolved (giant, bright giant, and supergiant) stars. The CDF gives the fraction of stars having a $V \sin i$ less than a specific upper value that ranges from zero to the maximum $V \sin i$ observed. The surprising result is that the distributions are very similar, with a slightly larger fraction of LMC stars rotating faster, but a slightly smaller fraction of SMC stars, with lowest Z , rotating slower than the Galactic stars. The two sample Kolmogorov-Smirnov (K-S) test compares two independent samples and determines a statistic, p describing the similarity of the CDFs. For low values of p ($\leq 5-10\%$), the null hypothesis that the two samples are drawn from the same parent population is rejected. Comparing the LMC and SMC samples with Galactic stars, their K-S p are 44% and 42%, respectively, indicating that they are drawn from the same parent population as the Galactic sample. Thus, there is no visible trend of CDFs with metallicity. The sample of unevolved (dwarf and subgiant) stars was too small to make a reliable comparison, but the average projected rotational velocities in each group appear to be comparable: $\langle V \sin i \rangle = 131 \pm 93$, 117 ± 31 , and 78 ± 45 km s $^{-1}$ for the Galactic, LMC, and SMC unevolved stars, respectively. The results of this study should be treated cautiously for two reasons. First, the samples of LMC and SMC targets are not large enough to assume a completely random distribution of inclination angle on the sky. Second, 18 of the HST/STIS SMC observations were obtained through one observing program. This program’s goal was to study the UV characteristics of massive stars at low Z . These targets may have a bias toward small projected rotational velocities, in order to better study the line depths as a function of metallicity.

Hillier et al. (2003) and Bouret et al. (2003) examined a total of 8 O-type stars in the SMC by fitting rotationally broadened synthetic spectra from the atmosphere model code TLUSTY (Hubeny & Lanz 1995) to the observed spectra. In all but one case the determined projected rotational velocities were ≤ 100 km s $^{-1}$, much smaller than the predicted equatorial rotation speeds of ≈ 200 km s $^{-1}$. There are several possible explanations: (1) the initial rotation rates may not be as large as 300 km s $^{-1}$ for massive stars in the SMC; (2) the stars may experience more spin down than predicted; and (3) with only 8 targets, the sample is just too small considering the random distribution of inclination.

The most recent survey of rotational velocities of O-type stars at low Z is a study by Mokiem et al. (2006), which is part of the larger VLT-FLAMES survey of massive stars (Evans et al. 2005). They determined $V \sin i$ values for 28 O-type stars in the SMC. A comparison of their unevolved targets (classes V, IV) to evolved targets (classes I, II, & III) shows that the unevolved sample contains relatively more fast rotators than the evolved stars. They point out that this trend is also seen in Galactic O type stars (Penny 1996; Howarth et al. 1997). New stellar interior models predict this behavior for solar metallicity stars but not for massive stars at $Z_{SMC} = 0.004$. They also compare their 21 unevolved SMC stars to 66 unevolved Galactic stars from Penny (1996). The K-S p is only 13%,

suggesting that there is a possible difference in the initial rotation rates of massive stars due to metallicity. However, Mokiem et al. (2006) warn that because of their small sample size, this result should be verified with a larger SMC sample.

All of the previous $V \sin i$ surveys of massive stars at low Z suffer from one common major fault, a small sample size. Here we present the results of our project to test the treatment of angular momentum in the new stellar interior models through a large scale survey of projected rotational velocities of O-type stars in three metallicity environments: the Milky Way ($Z_{MW} = 0.020$), LMC ($Z_{LMC} = 0.007$), and SMC ($Z_{SMC} = 0.004$). The Far Ultraviolet Spectrographic Explorer (FUSE) archive at the Multimission Archive at Space Telescope (MAST) contains spectra of 161 LMC and SMC stars with spectral classes between B2 - O2. The targets are 120 evolved (luminosity classes I, II, & III) and 41 unevolved (IV & V luminosity classes) stars in these low Z environments. In addition MAST contains spectra of approximately 100 Galactic O-type stars with known $V \sin i$ values. This is a large sample of O-type spectra, all observed with the same instrument. It contains both cluster and field stars. The observations were not part of any single campaign, in fact they were obtained through 38 different observing programs. These stars represent a completely uniform, unbiased sample. Comparisons of the $V \sin i$ distributions from the unevolved MC stars to similar classed Galactic stars will determine whether the initial rotation rates of massive stars have a metallicity dependence. Comparisons of the evolved stars in each environment to their unevolved counterparts will show whether the rotation rates are age dependent at that metallicity.

2. Projected Rotational Velocities from UV lines

For the extremely massive O-type stars, the major mechanisms that affect stellar line widths are rotation and macroturbulence. Conti & Ebbets (1977) completed the first large-scale survey of rotational velocities of Galactic O-type stars. They noted in their sample that no O-type star displayed extremely sharp lines that would be expected with a pole-on orientation and suggested that large-scale atmospheric motions contribute to the broadening of the spectral features. In determining their $V \sin i$ estimates they adopted the convention that only rotational broadening was present. They were aware this is not in general true and note, as do others who have adopted a similar convention (Penny 1996; Howarth et al. 1997), that their quoted $V \sin i$ is actually a parameter which is closely related to, but not necessarily, the exact projected equatorial velocities of the stars. Authors who have investigated the amount of macroturbulence present in early B-type supergiants have found values on the order of 20 –70 km s⁻¹ (Ryans et al. 2002; Dufton et al. 2006). These values do not

appear to be dependent upon metallicity as both the Galactic (Ryans et al. 2002) and the SMC (Dufton et al. 2006) samples result in similar values for macroturbulent broadening. While macroturbulence is undoubtedly a factor in the line widths of O-type stars, we can make a statistical argument that if each sample (Galactic, SMC, LMC) has the same contribution to line widths from macroturbulence, then the distribution of $V \sin i$ from each can be compared for differences in equatorial rotational velocities (see discussion in §5).

Our previous studies of projected rotational velocities (Penny 1996; Penny et al. 2004) utilized archival high-resolution spectra from the International Ultraviolet Explorer (IUE) and the Space Telescope Imaging Spectrograph (STIS) in the wavelength region 1200 – 1900 Å. The ultraviolet is actually a preferable region for determining projected rotational velocities for very massive stars. Unlike the photospheric lines seen in optical spectra, the UV lines are formed deeper in the star and are usually less contaminated by wind effects. Also there are thousands of lines present in the UV, compared to tens in the optical. The methodology used to obtain $V \sin i$ values from UV spectra differs from that used for optical spectra. We cross-correlate the spectrum of a narrow-lined star with that of a test star, which results in a cross-correlation function (CCF) that represents a “superline” of the test star. The superline will have an observed width related to the line width of the test star and that of the narrow-lined star. In the case of a double-lined binary, the CCF may display two peaks, which are separated by the radial velocity difference of the two stars. A calibration between CCF width and $V \sin i$ is obtained by cross-correlating a sample of stars with known projected rotational velocities.

3. Observations and Reductions

The CCF method can also be utilized with FUSE observations of O-type stars. We obtained FUSE archival spectra of 97 Galactic, 55 SMC, and 106 LMC massive stars that are available from MAST. For each star we obtain the calibrated (CALFUSE) exposure files from the LiF2 channel and detector segment A (hereafter LiF2A spectra). The LiF2A spectra cover only the wavelength region of 1086 – 1183 Å. Below this region the spectra are severely affected by interstellar features and are not suitable for our purpose. Each observation is actually composed of several exposures. The exposure spectra were extracted using the CALFUSE routine MRDFITS. Following this basic reduction we use a series of routines written in the Interactive Data Language¹ to further reduce the spectra. The extracted exposure spectra then were coadded with appropriate wavelength shifts, determined

¹IDL is a registered trademark of ITT Corporation

by cross-correlating the exposure with the highest flux value (reference spectrum) to all others, creating a weighted average spectrum based upon exposure lengths for each observation. These steps are consolidated into one routine COMBINE that writes the coadded spectrum to a file. Data spikes are removed in SPIKEOUT, which replaces any bad pixels with a median of surrounding pixels. One of the most important steps in this reduction is the placement of the data on a $\log \lambda$ grid, in which each pixel step corresponds to a uniform velocity step of 1 pixel = 10 km s⁻¹. This is done in the routine BINFUSE. The spectroscopic resolving power of the raw FUSE spectra is $20,000 \pm 2000$, however we further degrade this value by smoothing the data by a Gaussian transfer function (FWHM = 40 km s⁻¹) in GSMOOTH. Another important step is the alignment of all spectra of a star on the same wavelength system. In order to assure that all spectra of a given star are not shifted with respect to each other, the interstellar lines present (assumed to have a constant velocity) are used to align the system spectra. ISMALIGNFUSE does this by creating an average spectrum, cross-correlating the regions containing strong interstellar lines (which are picked interactively), and shifting each spectrum to an average wavelength grid. ISMALIGNFUSE also removes not only the strong interstellar features, but also those chosen (again, interactively) to be weak interstellar features. We cannot overemphasize the importance of removing the considerable number of interstellar lines, whose identification was greatly aided by earlier work of Barnstedt et al. (2000), Pellerin et al. (2002), and Walborn et al. (2002). The spectra are then rectified (routine FUSERECT) to a unit continuum, by fitting a spline function to a series of pseudo-continuum zones in an average spectrum and then dividing each of the spectra by the fit. The final spectral stacks are written to a file in WTSTKFUSE. All of these procedures are incorporated in a calling routine named MKSTKFUSE.

4. Projected Rotational Velocities from Cross-Correlation Functions

Target star spectra are cross-correlated with that of a relatively narrow-lined template star. Cross-correlation was done only in the wavelength regions 1100 – 1108 Å and 1130 - 1165 Å (1139 - 1165 Å, for stars with emission in the P V/ Si IV λ 1128 line), a region relatively free of wind features. While most of the lines in these regions are too weak and blended to identify individually, a few of the stronger features are O III λ 1149.6, 1150.9, 1153.8 Å, and S IV λ 1138.2 Å. The spectra are padded with 1000 km s⁻¹ of artificial continuum on both ends to include the entire observed range in the cross-correlation. The CCF is the sum of the square of the differences between the test spectrum and the reference spectrum shifted in velocity from –1000 km s⁻¹ to +1000 km s⁻¹ at 10 km s⁻¹ intervals. The functions are then rectified, inverted, and Gaussian fitted to obtain an estimate of the full-width at half-maximum (FWHM). In Figure 2 we present fitted CCFs for 4 Galactic targets, HD 46202,

HD 152233, HD 96917, and HD 41161 that were all made with the template spectrum of star AV 327 (O9.7 II-Ibw). We note that the ‘bumps’ present in the CCF of HD 41161 are typical for massive stars with large projected rotational velocities and are possible indicators of non-radial pulsations present in the star.

The next step is developing a calibration of CCF width to $V \sin i$ using the Galactic targets. These stars have known $V \sin i$ values from Howarth et al. (1997). We created calibrations for two template stars AV 327 (O9.5 II-Ibw) and SK -66 100 (O6 II(f)) in order to cover the large range in spectral class of our targets. These are presented in Figure 3. Because of the early type of SK -66 100, seven of the latest type stars did not produce significant CCF peaks and were not used to create the calibration for this template. In Table 1, we list the Galactic targets along with their spectral classes, $V \sin i$ values from Howarth et al. (1997), $V \sin i$ values computed from the calibrations of each template star, and the FUSE observations used. Spectral classes are as listed in Howarth et al. (1997).

For each target from the Magellanic Clouds, we follow a similar procedure. All targets are cross-correlated with both templates to determine which template creates the CCF with the highest peak. For target stars with more than one spectrum, each spectrum’s CCF is examined to determine if the peak is stationary. A CCF peak that moves from observation to observation is indicative of a single-lined spectroscopic binary, as in the case of NGC346-MPG324 which shows a peak shift of 110 km s^{-1} between two observations. In these cases, each CCF is fit individually. For targets with more than one observation and stationary peaks, the average CCF is fitted. A few of the stars’ CCFs had double peaks, indicating that they were double-lined spectroscopic binaries. These CCFs were fit with a double Gaussian. Then using the calibrations developed above a $V \sin i$ value is determined from the Gaussian width of each fitted CCF. In Tables 2 and 3 we list the SMC and LMC targets, their spectral classifications, $V \sin i$ values from this paper, along with any previous values, the template star utilized, FUSE observations, and an additional column for other comments. For those CCF with two peaks the weaker peak’s $V \sin i$ is given in parentheses. In Figure 4 we plot our $V \sin i$ values versus those from Mokiem et al. (2006, 2007) and Penny et al. (2004) for those targets in common. From the scatter in Figure 4, we estimate that the typical errors for our $V \sin i$ values are 10 km s^{-1} .

5. Results and Conclusions

We can compare the projected rotational velocity distributions of the different groups of stars by calculating their cumulative distribution function (CDF). Again, the CDF gives the fraction of stars having a $V \sin i$ less than a specific upper value that ranges from zero to

the maximum $V \sin i$ observed. Not all of our target stars are used in compiling the CDF. Stars with a ‘NO’ in the final column of Tables 2 and 3 are excluded from our analysis for various reasons. For the B-type stars in our sample, we perform an additional analysis to determine: if they formed from stars with initial masses larger than $15 M_{\odot}$, and the fraction of their current radii to their TAMS radii. For all the stars we also wish to insure that extremely close binary systems are not present. We calculate M_{bol} from their V , $B - V$ values, the $(B - V)_0$ calibration of Shull & van Steenberg (1985), $A_V = 3.1 \times E(B - V)$, bolometric corrections of Howarth & Prinja (1989), and a distance modulus of 18.3 and 19.1, for the LMC and SMC respectively. We adopt the effective temperatures from the calibration of Howarth & Prinja (1989) for O-types and Bohm-Vitense (1981) for B-types. From the evolutionary tracks of Schaerer et al. (1993), we extrapolate initial masses, current masses, $\log g$, current radii, and TAMS radii. As we expected a large number of our B-type targets are inappropriate for our analysis. None of the B-stars have initial masses smaller than $15 M_{\odot}$. However, thirty-six targets (11 SMC and 25 LMC) are a factor of 50% or more larger than their TAMS radii. The lack of lower mass B-type supergiants almost certainly reflects their lower luminosities and the subsequent difficulty of obtaining FUSE spectra of those stars. For the entire FUSE sample we also compare the interpolated $\log g$ values with the luminosity class for discrepancies which might indicate that more than one star is present in the spectrum. For our analysis we also include 27 SMC and 26 LMC stars from Mokiem et al. (2006, 2007) and Penny et al. (2004). We have already shown in Figure 4 that there are no systematic differences between the $V \sin i$ values from our FUSE analysis and those presented in these prior studies. These additional stars are presented in Tables 4 and 5, along with the spectral classification given in Mokiem et al. (2006, 2007) or Penny et al. (2004), and those authors’ $V \sin i$ values.

We divide the data into the following samples: SMC unevolved (32 stars), SMC evolved (19 stars), LMC unevolved (36 stars), and LMC evolved (42 stars). We also create samples for Galactic unevolved (79 stars) and evolved (56 stars) from Howarth et al. (1997). Following the convention of earlier studies (Penny 1996; Howarth et al. 1997; Penny et al. 2004; Mokiem et al. 2006, 2007), unevolved refers to stars with luminosity classes V & IV, while luminosity classes I & II are termed evolved. Class III stars are omitted from both groups. Three stars are without explicit luminosity classes, AV 80, SK -67 266, and SK -69 279, and we assign these to the evolved category based on the notes from their listed spectral classification source. For each sample we create a CDF and plot these in comparison with other samples to determine the similarity. For each comparison a K-S statistic, D , and its corresponding probability, p , are calculated and these are presented in Table 6. The test statistic, D , is the maximum vertical variance between the two CDFs at any $V \sin i$ value. The p value tells us the probability of obtaining a D value at least as extreme as

was observed, assuming that the two samples are drawn from the same parent population. So in cases where the p statistic is small, i.e., $\leq 5\%$, we can say that the probability of finding such a large D between two samples that are drawn from identical populations is very small. Plots of the comparisons made are presented in Figures 5 – 7 and 9 – 10. At the suggestion of the referee, we determined the mass distribution of each of our samples. For the MC stars, we adopted the current evolutionary masses extrapolated from the M_{bol} and T_{eff} analysis described in the paragraph above. Mass estimates for the Galactic sample can be found in Howarth & Prinja (1989). The mean masses of the samples are 37.8, 45.7, and $34.4M_{\odot}$ for the unevolved stars of the Galaxy, LMC, and SMC, respectively, and the means are systematically higher among the evolved stars of the same three environments, 45.4, 47.4, and $40.3M_{\odot}$, respectively. This difference is expected since the evolved O-star samples will be biased towards higher masses (the advanced evolutionary stages of lower mass stars occur at cooler temperatures). The K-S test indicates that the three evolved sets have statistically indistinguishable mass distributions. On the other hand, the K-S test suggests that some differences may exist among the unevolved star mass distributions (particularly between the SMC and LMC samples where $p = 0.7\%$), but given the relative small sample sizes, we doubt that these are significant.

First we examine the evolved and unevolved Galactic samples to determine the level of difference we would expect in an environment where the stars do slow down as they evolve (Fig. 5). We see that the maximum variance in their CDF is 0.30 and this occurs at $V \sin i$ of 83 km s^{-1} . This large a D value results in a p of 0.5%, but we should not be misled by this low value. At these smaller velocities the source of the difference between the evolved and unevolved samples is not a result of angular momentum loss, but from the larger amount of macroturbulence that is present in the evolved stars' photospheres, broadening their line profiles. At the higher velocities where we expect to see evidence of spin down, the largest divergence is ≈ 0.12 , which would give us a significantly higher p of 71%. This is not say that the evolved stars in the Galactic sample have not slowed down, but that this effect may be more subtle than we originally expected.

In the LMC, the same comparison of unevolved to evolved stars has a very different appearance (Fig. 6). The CDF of both samples appear very similar, and the derived $D = 0.15$ and corresponding $p = 75\%$ supports the null hypothesis that both are drawn from the same parent distribution. This result is in agreement with the suggestion of Wolff et al. (2008), using data from Hunter et al. (2008), that massive stars in the LMC have similar $V \sin i$ distributions regardless of their $\log g$ values. Examining Figure 6, we notice that there is almost no divergence at low $V \sin i$ values, and a smaller variance at larger $V \sin i$ than we see in the Milky Way samples. The very high p value here is primarily due to the presence of slow rotators among both the unevolved and evolved samples, unlike the Galactic evolved

group. At high $V \sin i$ values, the CDFs of evolved to unevolved differ by ≈ 0.09 which is only slightly smaller than the value for the Galactic samples. It is at the low velocity end of the CDF where the LMC samples differ from those of the Galactic samples. The good agreement between the low ends of the two CDFs for the LMC stars suggests that development of macroturbulence with evolution is not as large a factor in the photospheres of the massive stars in that environment and that the processes that lead to macroturbulent broadening may have a metallicity dependence.

The CDFs of the same populations in the SMC are presented in Figure 7. Although the p value from the KS test is 23%, which would indicate that the samples are drawn from the same parent population, the maximum difference D is 0.29, which is very close to that from the Galactic samples. The larger p value from the similar D reflects the much smaller sample sizes in the SMC. At the high velocity end of the CDF, the fraction of evolved stars with $V \sin i$ above 200 km s^{-1} is 11% compared to 13% for the unevolved. This does support the hypothesis that stars at SMC metallicity will not slow down as they evolve on the MS. At the other end of the CDF, there is a slightly larger fraction of unevolved stars with $V \sin i$ below $\approx 70 \text{ km s}^{-1}$, but this difference is much smaller than we see in the Galactic comparison. The real divergence between the evolved and unevolved CDFs comes at the intervening velocities. The maximum divergence, 0.29, occurs at $V \sin i = 107 \text{ km s}^{-1}$. The fractions of stars with $V \sin i$ at or below this value for the evolved and unevolved samples are 0.84 and 0.55, respectively. This trend was also seen by Mokiem et al. (2006), who surmised that the initial rotational velocity distribution in the SMC might vary significantly from that in the Galaxy. Why we see a disparity in the CDFs of the evolved and unevolved samples in between $80 - 190 \text{ km s}^{-1}$ only in the SMC samples is not clear. We emphasize that the K-S test results accept the null hypothesis that the unevolved and evolved samples in the SMC are drawn from the same parent distribution.

A primary purpose of this project is to examine observationally the amount of angular momentum loss during the MS lifetimes of massive stars and the effects of metallicity on this loss. Comparing the evolved to unevolved samples in Figures 5-7, we see that the D statistic at high $V \sin i$ values range from 0.12, 0.09, 0.02 in the Galaxy, LMC, and SMC, respectively. Taken by itself this is suggestive of a trend with decreasing Z . However, for the LMC and SMC comparisons, D statistics of 0.09 and 0.02 result in p values of 99.6% and 100%, indicating there is no statistical difference between the evolved and unevolved CDFs at high $V \sin i$. But this is also true in the Galaxy where we do expect to see the significant spin down between the evolved and unevolved samples. Here the corresponding p for a D of 0.12 is 71%, far above the 5% cutoff. Statistically the loss of angular momentum for these H-burning stars is not so different between these three metallicity environments.

Although our results may appear to cast doubt on the rotational evolution predicted by models, we suspect that the rather small changes we find are probably consistent with models. Unfortunately, at the moment there are no large grids available for rotational evolution that might be used to compare with our statistical results. The best set was calculated by Ekström et al. (2008) who present evolutionary tracks for model 20 and $60M_{\odot}$ stars. The tracks for the $20M_{\odot}$ models are not immediately applicable since their portions that correspond to luminosity classes I and II occur in the cooler B-star domain (not included in our sample statistics). On the other hand, the tracks for $60M_{\odot}$ stars probably only apply to a small fraction of our sample of stars. However, the $60M_{\odot}$ tracks do cover all luminosity classes, so we can use them to make a representative comparison of the predicted and observed changes in rotational velocity with age. We plot in Figure 8 the $60M_{\odot}$ models from Ekström et al. (2008) that show the change in the average $V \sin i$ with age. Here we have multiplied the model equatorial velocities by a factor of $\pi/4$ to represent the average projected velocity for random orientations. The thin solid lines show the velocity evolution for Galactic abundance stars for three values of the initial ratio of actual to critical angular velocity, and the thin dotted lines show the same for lower metallicity SMC stars. Above these are three tick marks indicating those ages associated with luminosities and temperatures of luminosity class V, III, and I stars according to the observational calibration of Martins et al. (2005). For simplicity, we will assume that our sample groups of stars correspond to ages midway between 1 Myr (approximately when massive stars emerge from their natal, ultracompact H II region) and 1.83 Myr (the class III age) for the unevolved group and midway between 1.83 Myr and the age at which they cool to $T_{\text{eff}} = 28$ kK (the boundary between O- and B-supergiants) for the evolved group. We plot our derived average $V \sin i$ values for these groups (Table 6) versus their assigned mid-ages (relative to the $60M_{\odot}$ tracks) as thick solid and dotted lines bounded by plus signs for the Galactic and SMC samples, respectively. We see that the modest declines observed are not too different from the model estimates for stars with relatively small rotational velocities. The tracks for lower mass stars are qualitatively similar, but their later, evolved portions where the rotational velocities change the most will be progressively shifted out of the O-star domain into cooler classes, so that the predicted changes in mean rotational velocity between unevolved and evolved samples will be even smaller than shown in Figure 8. Thus, we emphasize that our simple comparison is probably only valid for considering relative trends with age and metallicity, and a detailed comparison would require additional tracks for other masses and sampling of the tracks based upon the observed mass and $V \sin i$ distributions.

We also are interested in whether the initial $V \sin i$ distribution is the same in the three environments. In Figure 9, we plot the CDFs of all three dwarf samples. Statistically all three have p values that are above the cut-off of 5%, and certainly at the high $V \sin i$ end all three

look extremely similar, indicating that the maximum rotational velocities are very similar. Below 200 km s^{-1} , the behavior of the three distributions varies. Again we see that the shape of the CDF for the SMC dwarfs is dissimilar from that of the counterparts in the Galaxy and the LMC between $80 - 190 \text{ km s}^{-1}$. Below 80 km s^{-1} , the fraction of slowly rotating stars varies between the three environments, with the Galactic sample in between the SMC and LMC. In fact the largest divergence between the LMC and SMC CDFs comes at $V \sin i \approx 65 \text{ km s}^{-1}$, resulting in a p value just above the statistically significant level. Hunter et al. (2008) showed an analogous plot, but for objects with $M < 25M_{\odot}$. Similarly they find good agreement between the LMC and Galactic samples, with the SMC sample lying slightly beneath the other two, especially in the region below 200 km s^{-1} . It is interesting that there are no very slow rotators in our LMC dwarf sample. At these low velocities, the dominating effect must not depend upon metallicity since the Galaxy’s metallicity, with significantly higher Z , is situated between that of the two low Z samples. We conclude that the initial velocity distribution in our three unevolved samples are statistically indistinguishable.

Finally we compare the evolved stars in each environment to examine the relative fractions of stars with large $V \sin i$ (Fig. 10). Looking at the distributions at the high velocity end, we see that a slightly larger fraction of evolved stars in the SMC have $V \sin i$ values larger than 200 km s^{-1} than in the Galaxy or LMC, which might support theoretical predictions. But the large D values that are found between the LMC and SMC samples are again at the low velocity range, $\approx 80 \text{ km s}^{-1}$. The maximum differences between the Galaxy and both the LMC and SMC CDFs occur near this velocity, with both of the low metallicity environments having a larger fraction of stars with smaller values compared to the Milky Way sample. In fact the trend is very supportive of our earlier suggestion that metallicity plays an important role in macroturbulent broadening in evolved O-type stars. A recent paper by Cantiello et al. (2008) discusses the origin of atmospheric turbulence in massive stars by sub-surface convection zones that are driven by Fe-peak element ionizations. In their simulations, the threshold luminosity for the occurrence of an iron convective zone is ten times lower at Z_{MW} than that for Z_{SMC} . Our results support their prediction that turbulence will increase with metallicity. The SMC evolved sample has the largest fraction of slow rotators, followed by the LMC and then the Galaxy. We note that the D values for the SMC vs. Galaxy and LMC vs. Galaxy are extremely similar, but result in differing p values owing to the smaller SMC sample size. The large divergence at small $V \sin i$ values between the Galaxy and LMC, and possibly SMC, leads us to reject the hypothesis that they are both from the same parent distribution. Again we stress that the differences that cause this are not the fractions of stars with large $V \sin i$, but those with small values.

In conclusion, we find some support for the new stellar interior model predictions that massive stars in lower metallicity environments will remain at almost constant rotation rates

throughout their MS lifetimes. But we also see that this effect, loss of angular momentum during the MS, is more subtle than previously reported even at the higher Galactic metallicity. We find that the ratio of mean $V \sin i$ in the evolved to unevolved samples is 0.84, 0.90, and 0.88 for the O-stars of the Galaxy, LMC, and SMC, respectively. This is consistent with the general expectation of spin down and the specific expectation that the spin down rates are large in the Galaxy where mass loss rates are higher. Note that the ratio of 0.84 for the Galaxy is an upper limit, since the apparent projected velocities of the Galactic evolved stars are systematically higher because of larger macroturbulence. With the exception of the SMC unevolved sample, the largest divergence between sample CDFs occur at low $V \sin i$ values. We have suggested that metallicity may play an important role in the development of macroturbulence in the photospheres of the evolved, massive stars. Finally, we once again see that small sample sizes, particularly for the SMC, hamper our ability to establish the true distribution of equatorial rotational velocities. We urge the continued observational efforts to determine the $V \sin i$ values for a large number of massive stars in differing Z environments to address this pressing and important issue.

The FUSE data presented in this paper were obtained from the Multimission Archive at the Space Telescope Science Institute (MAST). STScI is operated by the Association of Universities for Research in Astronomy, Inc., under NASA contract NAS 5-26555. Support for MAST for non-HST data is provided by the NASA Office of Space Science via grant NAG 5-7584 and by other grants and contracts. This research has made use of the SIMBAD database, operated at CDS, Strasbourg, France. Support for this work was provided by program GO63 from FUSE and NASA 06-ADP06-68. Institutional support for L.R.P. has been provided from the College of Charleston School of Sciences and Mathematics. Additional support for L.R.P. was provided from AR Nos. 09945 and 11275 from STScI, NASA grant NAG 5-2979, and NSF grant AST-0506541. Additional support for D.R.G. was provided by the National Science Foundation under Grant No. AST-0606861. We gratefully acknowledge all this support.

APPENDIX: NOTES ON INDIVIDUAL STARS

AV 80 – This star is included in the CDF for SMC evolved stars in accord with the individual notes in Walborn et al. (2000), who state that its absolute visual magnitude and the strength of its UV wind features correspond to a luminosity class of III.

AV 177 – The CCF has a double-peaked appearance, however the velocity separation is not large enough for a double Gaussian fit. The $V \sin i$ value listed is of both peaks together.

AV 332 – Known as a double-lined spectroscopic binary classified as WN3 + O6.5 I (Massey et al. 2000). Only one peak is seen in the CCFs, probably that of the O6.5 I component, which moves in V_r by 45 km s^{-1} between the observations taken 6 months apart.

AV 476 – Classified as O2-3 V + companion by Massey et al. (2005), we see two peaks, separated by V_r of 363 km s^{-1} .

NGC346-MPG324 – The peak in the two observations moves by 110 km s^{-1} and changes width.

SK -65 21 – There are four observations taken in sequence over 15 hours. All CCFs show double peaks that appear to be near or at maximum velocity separation of 350 km s^{-1} . The peaks first move slightly farther apart and then closer over the four observations.

SK -66 172 – Classified as O2 III(f*) + OB (Walborn et al. 2002), we do not see any sign of a companion in the CCF.

SK -67 18 – Koenigsberger et al. (2003) classified this system as O3 + O8-B0 I. We see both peaks in the CCF.

SK -67 166 – Observed 63 times with FUSE over approximately a 5 week period, the peak does not move.

SK -68 52 – A weak second peak is stronger in the CCF with AV327 than with SK -66 100. The peaks are separated by 350 km s^{-1} .

SK -69 94 – The FUSE spectrum of S Dor is contaminated by the visual companion $13''$ away which is classified as a B1 I (Wolf et al. 1980). The CCF here is almost certainly representative of this star, not S Dor.

SK -69 223 – Classified WC4(+OB) by Bartzakos et al. (2001), we do not see any sign of a second peak in the CCFs. However the main peak does move slightly between the two available observations taken 50 minutes apart.

SK -70 91 – Classified a O2 III(f*) + OB by Walborn et al. (2002), both stars have peaks in CCF. The peaks are separated by 255 km s^{-1} .

BI 173 – In the two observations taken two months apart, the main peak moves by 53 km s^{-1} . There is a low level second peak, but it is difficult to distinguish it from the surrounding noise.

HV 2241 – A known binary, we do not see any sign of the secondary, classified as early B (Mokiem et al. 2006), in the CCF.

LMC X-4 – This spectrum is of the O8 III companion in this X-ray binary.

PGMW 3209 – Only one extremely noisy observation is available from FUSE. We do not see any sign of a second peak in the CCF.

REFERENCES

- Barnstedt, J., Gringel, W., Kappelman, N., & Grewing, M. 2000, *A&AS*, 143, 193
- Bartzakos, P., Moffat, A. F. J., & Niemela, V. S. 2001, *MNRAS*, 324, 33
- Bohannon, B., & Walborn, N. R. 1989, *PASP*, 101, 520
- Bohm-Vitense, E. 1981, *ARA&A*, 19, 295
- Bouret, J.-C., Lanz, T., Hillier, D. J., Heap, S. R., Hubeny, I., Lennon, D. J., Smith, L. J., & Evans, C. J. 2003, *ApJ*, 595, 1182
- Cantiello, M., Langer, N., Brott, I., de Koter, A., Shore, S. N., Vink, J., Voegler, A., & Yoon, S. C. 2008, arXiv:0810.2546
- Conti, P. S., & Ebbets, D. 1977, *ApJ*, 213, 438
- Conti, P. S., Garmany, C. D., & Massey, P. 1986, *AJ*, 92, 48
- Courtes, G., Viton, M., Bowyer, S., Lampton, M., Sasseen, T. P., & Wu, X.-Y. 1995, *A&A*, 297, 338
- Crampton, D., & Greasley, J. 1982, *PASP*, 94, 31
- Crowther, P. A., Hillier, D. J., Evans, C. J., Fullerton, A. W., De Marco, O., & Willis, A. J. 2002, *ApJ*, 579, 774
- Dufton, P. L., Ryans, R. S. I., Simón-Díaz, S., Trundle, C., & Lennon, D. J. 2006, *A&A*, 451, 603
- Ekström, S., Meynet, G., Maeder, A., & Barblan, F. 2008, *A&A*, 478, 467
- Evans, C. J., Howarth, I. D., Irwin, M. J., Burnley, A. W., & Harries, T. J. 2004, *MNRAS*, 353, 601
- Evans, C., Smartt, S., Lennon, D., Dufton, P., Hunter, I., Mokiem, R., de Koter, A., & Irwin, M. 2005, *The Messenger*, 122, 36

- Fehrenbach, C., & Dufflot, M. 1982, *A&AS*, 48, 409
- Fitzpatrick, E. L. 1988, *ApJ*, 335, 703
- Fitzpatrick, E. L. 1991, *PASP*, 103, 1123
- Fitzpatrick, E. L., & Garmany, C. D. 1990, *ApJ*, 363, 119
- Garmany, C. D., Conti, P. S., & Massey, P. 1987, *AJ*, 93, 1070
- Gummersbach, C. A., Zickgraf, F.-J., & Wolf, B. 1995, *A&A*, 302, 409
- Heger, A. & Langer, N. 2000, *ApJ*, 544, 1016
- Hillier, D. J., Lanz, T., Heap, S. R., Hubeny, I., Smith, L. J., Evans, C. J., Lennon, D. J., & Bouret, J. C. 2003, *ApJ*, 588, 1039
- Howarth, I. D., & Prinja, R. K. 1989, *ApJS*, 69, 527
- Howarth, I. D., Siebert, K. W., Hussain, G. A. J., & Prinja, R. K. 1997, *MNRAS*, 284, 265
- Hunter, I., Lennon, D. J., Dufton, P. L., Trundle, C., Simón-Díaz, S., Smartt, S. J., Ryans, R. S. I., & Evans, C. J. 2008, *A&A*, 479, 541
- Hubeny, I., & Lanz, T. 1995, *ApJ*, 439, 875
- Jaxon, E. G., Guerrero, M. A., Howk, J. C., Walborn, N. R., Chu, Y.-H., & Wakker, B. P. 2001, *PASP*, 113, 1130
- Keller, S. C. 2001, *PASP*, 113, 1570
- Koenigsberger, G., Moffat, A. F. J., & Auer, L. H. 2003, *Revista Mexicana de Astronomia y Astrofisica*, 39, 213
- Maeder, A., Grebel, E. K., & Mermilliod, J.-C. 1999, *A&A*, 346, 459
- Maeder, A., & Meynet, G. 2001, *A&A*, 373, 555
- Martins, F., Schaerer, D., & Hillier, D. J. 2005, *A&A*, 436, 1049
- Massey, P. 2002, *ApJS*, 141, 81
- Massey, P., Lang, C. C., Degioia-Eastwood, K., & Garmany, C. D. 1995, *ApJ*, 438, 188
- Massey, P., Puls, J., Pauldrach, A. W. A., Bresolin, F., Kudritzki, R. P., & Simon, T. 2005, *ApJ*, 627, 477

- Massey, P., Waterhouse, E., & DeGioia-Eastwood, K. 2000, *AJ*, 119, 2214
- Meynet, G. & Maeder, A. 2000, *A&A*, 346, 459
- Mokiem, M. R., et al. 2006, *A&A*, 456, 1131
- Mokiem, M. R., et al. 2007, *A&A*, 465, 1003
- Negueruela, I., & Coe, M. J. 2002, *A&A*, 385, 517
- Ostrov, P. G., Morrell, N. I., & Lapasset, E. 2001, *A&A*, 377, 972
- Parker, J. W., Garmany, C. D., Massey, P., & Walborn, N. R. 1992, *AJ*, 103, 1205
- Pellerin, A., et al. 2002, *ApJS*, 143, 159
- Penny, L. R. 1996, *ApJ*, 463, 737
- Penny, L. R., Gies, D. R., & Bagnuolo, W. G. 1999, *ApJ*, 518, 450
- Penny, L. R., Sprague, A. J., Seago, G., & Gies, D. R. 2004, *ApJ*, 617, 1316
- Plante, J. 1998, M.Sci. Thesis, Univ. Laval
- Robert, C., Pellerin, A., Aloisi, A., Leitherer, C., Hoopes, C., & Heckman, T. M. 2003, *ApJS*, 144, 21
- Rousseau, J., Martin, N., Prévot, L., Rebeiro, E., Robin, A., & Brunet, J. P. 1978, *A&AS*, 31, 243
- Ryans, R. S. I., Dufton, P. L., Rolleston, W. R. J., Lennon, D. J., Keenan, F. P., Smoker, J. V., & Lambert, D. L. 2002, *MNRAS*, 336, 577
- Schaerer, D., Charbonnel, C., Meynet, G., Maeder, A., & Schaller, G. 1993, *A&AS*, 102, 339
- Schaller, G., Schaerer, D., Meynet, G., & Maeder, A. 1992, *A&AS*, 96, 269
- Shull, J. M., & van Steenberg, M. E. 1985, *ApJ*, 294, 599
- Smith Neubig, M. M., & Bruhweiler, F. C. 1997, *AJ*, 114, 1951
- Smith Neubig, M. M., & Bruhweiler, F. C. 1999, *AJ*, 117, 2856
- Walborn, N. R. 1977, *ApJ*, 215, 53

Walborn, N. R., Lennon, D. J., Haser, S. M., Kudritzki, R.-P., & Voels, S. A. 1995, *PASP*, 107, 104

Walborn, N. R., Lennon, D. J., Heap, S. R., Lindler, D. J., Smith, L. J., Evans, C. J., & Parker, J. W. 2000, *PASP*, 112, 1243

Walborn, N. R., Fullerton, A. W., Crowther, P. A., Bianchi, L., Hutchings, J. B., Pellerin, A., Sonneborn, G., & Willis, A. J. 2002, *ApJS*, 141, 443

Wolf, B., Appenzeller, I., & Cassatella, A. 1980, *A&A*, 88, 15

Wolff, S. C., Strom, S. E., Cunha, K., Daflon, S., Olsen, K., & Dror, D. 2008, *AJ*, 136, 1049

Table 1. Galactic Targets

Star	Spectral Classification	$\langle V \sin i \rangle$			FUSE data set
		Howarth et al. (1997) (km s ⁻¹)	AV 327 (km s ⁻¹)	SK -66 100 (km s ⁻¹)	
HD 108	O6:f?pe	78	66	82	O63508010
HD 5005A	O6.5 V((f))	99	78	108	P1020102
HD 12323	ON9 V	131	99	73	P1020202
HD 13268	ON8 V	309	264	252	P1020304
HD 14134	B3 Ia	66	85	...	D9021001
HD 14434	O5.5 Vn((f))p	423	412	436	P1020504
HD 15642	O9.5 III:n	331	398	...	M1122301, P1020702
HD 34078	O9.5 V	30	45	54	A0700203, B0630102, C0730101-2, E0760101
HD 34656	O7 II(f)	91	70	75	P1011301
HD 41161	O8 Vn	304	314	353	P1021001
HD 42088	O6.5 V	65	68	66	P1021101
HD 45314	OBe	285	308	227	P1021301
HD 46056	O8 Vn	330	274	310	P1160901
HD 46149	O8.5 V	78	75	66	C1680401
HD 46150	O5 V((f))	111	78	88	C1680201, P1021401-3
HD 46202	O9 V	37	43	46	P1161001
HD 46223	O4 V((f))	82	68	114	C1680302
HD 60369	O9 IV	67	74	62	P1050201
HD 61347	O9 Ib	116	98	106	P1022001-2
HD 63005	O6 V((f))	74	72	98	P1022101
HD 69106	B0.5 IVnn	325	309	353	P1022301-2
HD 72648	B2.5 II-III	48	45	...	A1290401
HD 74920	O7 III:n	251	298	286	P1022601
HD 89137	ON9.7 III(n)p	202	231	137	P1022801
HD 90087	O9.5 III	272	305	259	P3030401, P1022901
HD 91572	O6 V((f))	62	67	75	P3031701
HD 91651	O9 V:n	292	318	294	P1023101-2
HD 91824	O7 V((n))	65	69	70	A1180802
HD 92554	O9.5 II:n	298	348	308	P1023201-2
HD 92850	O9.5 Ib	78	61	53	P3031601
HD 93028	O9 V	42	65	49	A1180902
HD 93146	O6.5 V((f))	79	83	78	P1023301
HD 93222	O7 III((f))	77	87	81	P1023701
HD 93249	O9 III	78	69	71	Z9013401
HD 93250	O3 V((f))	107	162	129	P1023801
HD 93843	O5 III(f) var	95	96	104	P1024001
HD 96670	O8 p	139	111	120	P1024201
HD 96715	O4 V((f))	76	75	96	P1024301
HD 96917	O8.5 Ib(f)	176	178	178	P1024401
HD 99546	O8	79	68	65	P3031901
HD 100444	O9 Ib	83	72	75	Z9014101
HD 101008	O9 IV	60	67	47	Z9014201
HD 101190	O6 V((f))	88	83	118	P1025001
HD 101298	O6 V((f))	80	79	95	P1025201

Table 1—Continued

Star	Spectral Classification	$\langle V \sin i \rangle$			FUSE data set
		Howarth et al. (1997) (km s ⁻¹)	AV 327 (km s ⁻¹)	SK -66 100 (km s ⁻¹)	
HD 101413	O8 V	99	94	90	P1025301
HD 101436	O6.5 V	98	127	128	P1025401
HD 102475	B0.5 II	56	65	53	G0630301
HD 104683	B1 Ib	59	48	...	Z9014401
HD 105056	ON9.7 lae var	68	70	58	Z9014501
HD 111973	B3 Ia	68	73	...	Z9014501
HD 112784	O9.5 III	51	58	51	Z9015001
HD 113012	B0.2 Ib	51	58	48	Z9015101
HD 115455	O7.5 III((f))	69	84	85	A1200701
HD 116852	O9 III	136	114	95	P1013801
HD 122879	B0 Ia	92	69	58	B0710501
HD 124314	O6 V(n)((f))	242	285	302	P1026201
HD 124979	O8 ((f))	220	252	280	P1026301
HD 148937	O6.5 f?p	76	77	90	C1680101
HD 152233	O6 III:(f)p	104	102	102	P1026702
HD 152249	OC9.5 Iab	99	83	72	B0250401
HD 152314	O9.5 III-IV	76	86	72	P1026901
HD 152405	O9.7 Ib-II	77	68	56	P3031801
HD 152424	OC9.7 Ia	86	74	67	Z9016301
HD 152590	O7.5 V	60	76	76	B0710601-2
HD 152623	O7 V(n)((f))	106	97	94	P1027001
HD 152723	O6.5 III(f)	111	104	107	P1027102
HD 154368	O9.5 Iab	102	89	78	P1161901
HD 157857	O6.5 III(f)	97	99	151	P1027501
HD 163758	O6.5 Iaf	90	84	83	P1015901
HD 163892	O9 IV((n))	201	287	254	P1027601-2
HD 167659	O7 II(f)	85	77	95	P1028001
HD 168076	O4 V((f))	98	77	116	P1162201
HD 168941	O9.5 II-III	116	96	82	P1016501-2
HD 175754	O8 II((f))	177	207	193	P1016802
HD 175876	O6.5 III(n)(f)	266	274	293	P1016902
HD 186890	O7.5 III((f))	83	88	85	P3030201
HD 189957	O9.5 III	92	92	78	P3030301
HD 190429A	O4 If+	105	77	73	P1028401
HD 190864	O6.5 III(f)	88	85	91	E0820501
HD 191423	O9 III:n*	436	356	336	P3030101, E0821301
HD 192639	O7 Ib(f)	96	110	100	C1710101, P1162401
HD 193514	O7 Ib(f)	94	94	94	E0820701
HD 199579	O6 V((f))	73	70	82	P1162501
HD 201345	ON9 V	91	69	58	P1223001
HD 207198	O9 Ib-II	91	71	69	P1162801
HD 207538	O9.5 V	51	58	36	P1162902-3
HD 210809	O9 Iab	117	98	81	P1223101-3
HD 216532	O8.5 V((n))	189	225	123	A0510202

Table 1—Continued

Star	Spectral Classification	$\langle V \sin i \rangle$			FUSE data set
		Howarth et al. (1997) (km s ⁻¹)	AV 327 (km s ⁻¹)	SK -66 100 (km s ⁻¹)	
HD 217086	O7 Vn	332	310	343	E0820801
HD 218915	O9.5 Iab	94	75	74	P1018801
HD 225094	B3 Ia	68	77	...	Z9120101
HD 303308	O3 V((f))	111	85	137	P1221601-2
BD -48 3437	B1 Iab	54	44	...	P1018401-3
BD -60 2522	O6.5 (n)(f)p	178	249	228	D1130101
CPD -59 2600	O6 V((f))	142	135	182	P1221401-3
CPD -74 1569	O9.5 V	64	68	59	P1015301, U1092701

Table 2. SMC Targets

Star	Spectral Classification	Ref.	$\langle V \sin i \rangle$		Template Star	FUSE data sets	Notes
			This paper (km s ⁻¹)	Other (km s ⁻¹)			
AV 14	O3-4 V + neb	1	261	212 ^a	AV 327	P1175301	
AV 15	O6.5 II(f)	2	95	128 ^b 132 ^c 135 ^a	AV 327	P1150101	
AV 26	O7 III+neb	1	141	127 ^b 128 ^a	AV 327	P1176001	
AV 47	O8 III((f))	2	79	76 ^b 169 ^c	AV 327	P1150202	
AV 61	O5 III	3	228		SK -66 100	E5110201	
AV 69	OC7.5 III((f))	2	94	100 ^b 104 ^c	AV 327	P1150303	
AV 70	O9 Ia	3	62		AV 327	A1180202-3	
AV 75	O5 III(f+)	2	94	109 ^b 110 ^c	AV 327	P1150404	
AV 80	O4-6 n(f)p	2	278	324 ^b 270 ^c	AV 327	E5111701	*
AV 83	O7 Iaf+	2	71	82 ^b 80 ^c 70 ^f	AV 327	P1176201	
AV 95	O7 III((f))	2	76	82 ^b 89 ^c 68 ^a	AV 327	E0540101, P1150505	
AV 96	B1 Ia	3	70		AV 327	C1600101	NO
AV 104	B0 Ib	3	56		AV 327	D1260101	
AV 119	B2 II	1	48		AV 327	Z9122101	NO
AV 120	O9.5 III	4	70		AV 327	E5110301	
AV 175	B2 Iab	3	51		AV 327	Z9122001	NO
AV 177	O4 V	3	428		SK -66 100	C0020102	*, NO
AV 207	O7 V	1	75		AV 327	P1175901	
AV 210	B1.5 Ia	3	43	37 ^d	AV 327	D1620601	NO
AV 215	B0 Ia	3	92	66 ^d	AV 327	D1620401	
AV 216	B1 III:	3	83		AV 327	D1620501	
AV 232	O7 Iaf+	5	76	106 ^b 74 ^a	AV 327	P1030201	SK 80
AV 235	B0 Iaw	5	90		AV 327	P1030301	SK 82
AV 238	O9.5 III	5	71		AV 327	P1176601	
AV 242	B0.7 Iaw	5	83	54 ^d	AV 327	P1176901	NO
AV 255	O8 V	6	188		AV 327	E5110501	
AV 261	O8.5 I	6	87		AV 327	E5110601	
AV 264	B1 I	5	116		AV 327	P1177001	NO
AV 266	B1 I	3	61		AV 327	Z9122301	NO
AV 267	O8 V	7	268		AV 327	E5110701	
AV 321	O9 Ib	3	357		AV 327	P1150606	
AV 327	O9.7 II-Ibw	5	69	71 ^b 80 ^c	AV 327	P1176401	
AV 332	O6.5 I +WN3	8	90		AV 327	P1030401, X1050102	*,SK 108, NO
AV 372	O9 Iabw	5	98	135 ^a	AV 327	P1176501	
AV 374	B2 Ib	9	73	47 ^d	AV 327	C1600201	NO
AV 377	O6 V	1	51		AV 327	B1340101	
AV 378	O9 III	3	64		AV 327	P1150707	
AV 388	O4 V	1	147	163 ^a , 179 ^b	AV 327	P1175401	
AV 423	O9.5 II(n)	5	163	186 ^b	AV 327	P1176701	
AV 435	O4 V	6	96		AV 327	E5111601	
AV 440	O7 V	1	62		AV 327	E5110901	
AV 446	O6.5 V	1	124		AV 327	E5111001	
AV 456	O9.5 Ib	4	111		AV 327	Q1070101-4, 0106	SK 143
AV 462	B1.5 Ia	9	57	43 ^d	AV 327	A1180301	NO

Table 2—Continued

Star	Spectral Classification	Ref.	$\langle V \sin i \rangle$		Template Star	FUSE data sets	Notes
			This paper (km s^{-1})	Other (km s^{-1})			
AV 469	O8 II	1	79	81 ^a	AV 327	P1176301	
AV 472	B2 Ia	9	73	33 ^d	AV 327	C1600301	NO
AV 476	O2-3 V + comp	10	65(54)		AV 327	C0020301	*, NO
AV 488	B0.5 Iaw	11	87		AV 327	P1176801-3, P1030501	SK 159
NGC346-MPG324	O4 V((f))	5	74,118	70 ^b 120 ^c 105 ^a 70 ^e	AV 327	P2030502, P1175601	*, NO
NGC346-MPG342	O5-6 V	5	58		AV 327	P2030401, P1175701	
NGC346-MPG355	O2 III(f*)	5	112	112 ^b 120 ^c 110 ^e	SK -66 100	P1175201	
NGC346-MPG435	O4 III(n)(f)	5	93		AV 327	P2030201, P1175501	
SK 190	O8 Iaf	13	302		AV 327	E5111401	
SK 191	B1.5 Ia	9	118	92 ^d	AV 327	D1620201	NO
SK 197	O8.5 Ve	12	166		AV 327	E5111501	

Note. — Spectral Classifications from (1) Garmany et al. (1987), (2) Walborn et al. (2000), (3) Smith Neubig & Bruhweiler (1997), (4) Evans et al. (2004), (5) Walborn et al. (2002), (6) Massey et al. (1995), (7) Crampton & Greasley (1982), (8) Massey et al. (2000), (9) Dufton et al. (2006), (10) Massey et al. (2005), (11) Walborn et al. (1995), (12) Courtes et al. (1995), and (13) Massey (2002). $V \sin i$ values from (a) Mokiem et al. (2006), (b) Penny et al. (2004), (c) Walborn et al. (2000), (d) Dufton et al. (2006), (e) Bouret et al. (2003), (f) Hillier et al. (2003). *Additional notes on individual stars are presented in the Appendix.

Table 3. LMC Targets

Star	Spectral Classification	Ref.	$\langle V \sin i \rangle$		Template Star	FUSE data sets	Notes
			This paper (km s ⁻¹)	Other (km s ⁻¹)			
SK -65 01	B0.5 I	1	74		AV 327	A0490302	NO
SK -65 05	O9 II	2	153		AV 327	E5112301	
SK -65 21	O9.7 Iab	3	57(58)		AV 327	P1020901-4	*, NO
SK -65 22	O6 Iaf+	3	66		AV 327	P1031002	
SK -65 44	O9 V	4	132		AV 327	P11733301-2	
SK -65 47	O4 If	5	208		SK -66 100	C0020701	
SK -65 63	O9.7 I	6	77		AV 327	A0490701-2, B0861101, M1142001	
SK -66 01	B1.5 Ia	6	78		AV 327	C1600601	NO
SK -66 18	O6 V((f))	7	100	82 ^a	SK -66 100	A0490101-2	
SK -66 78	B1.5 I	1	65		AV 327	B1280301	NO
SK -66 97	B1 Iab	8	159		SK -66 100	E9570101	Hen S35, NO
SK -66 100	O6 II(f)	3	67	84 ^a	AV 327	P1172303	
SK -66 106	B2 Ia	6	78		AV 327	B1280901	NO
SK -66 118	B2 Ia	6	167		AV 327	C1600701	NO
SK -66 169	O9.7 Ia+	3	71	72 ^b	AV 327	P1173801	HD 269889
SK -66 171	O9 Ia	6	90		AV 327	E5114102	
SK -66 172	O2 III(f*)+OB	3	101		SK -66 100	P1172201	*, NO
SK -66 185	B0 Iab	2	53		AV 327	A0490902	
SK -67 05	O9.7 Ib	3	87		AV 327	P1030703-4	
SK -67 14	B1.5 Ia	3	88		AV 327	P1174201-3	NO
SK -67 18	O3 + O8-B0 I	9	80(67)		SK -66 100	D0980801	*, NO
SK -67 28	B0.7 Ia	6	76		AV 327	A0490201-2	NO
SK -67 38	O8.5 V	7	100		AV 327	E5112601	
SK -67 46	B1.5 I	1	71		AV 327	A0491501	NO
SK -67 69	O4 III(f)	3	121		SK -66 100	P1171701, 1703	
SK -67 76	B0 Ia	11	80		AV 327	P1031201	
SK -67 100	B1 Ia	6	88		AV 327	B1280401	HD 269504, NO
SK -67 101	O8 II((f))	3	103	101 ^b	AV 327	P1173401-3	
SK -67 106	B0 I	12	99	135 ^b	AV 327	A1110101	
SK -67 107	B0 I	13	82	103 ^b	AV 327	A1110201	
SK -67 111	O6 Ia(n)fp var	3	259	209 ^b	AV 327	C1550208-9, C1550214-5	
SK -67 118	O7 V	7	61		AV 327	E5113401	
SK -67 119	O7 III(f)	7	235		AV 327	E5113501	
SK -67 150	B1 Ia	4	66		AV 327	B1281001	NO
SK -67 166	O4 If+	3	97	157 ^b , 97 ^a	SK -66 100	A1330101-162, A1330180	*
SK -67 167	O4 Inf+	3	155		SK -66 100	P1171901-2	
SK -67 169	B1 Ia	3	62		AV 327	P1031603	NO
SK -67 174	O8 V	7	72		AV 327	D0980101	
SK -67 176	O7 Ib(f)	6	54		AV 327	D0980201	
SK -67 181	B0.5 I	11	99		AV 327	B0900101	NO
SK -67 191	O8 V	2	100		AV 327	P1173101-2	
SK -67 256	B1 Ia	6	66		AV 327	B1280201	NO
SK -67 266	Ofpe/WN9	14	113	144 ^b	SK -66 100	B0900201	
SK -68 03	O9 I	2	70		AV 327	A0490401-2	

Table 3—Continued

Star	Spectral Classification	Ref.	$\langle V \sin i \rangle$		Template Star	FUSE data sets	Notes
			This paper (km s ⁻¹)	Other (km s ⁻¹)			
SK -68 16	O7 III	2	100		AV 327	E5112201	
SK -68 41	B0.5 Ia	6	77		AV 327	P1174101-2	NO
SK -68 52	B0 Ia	3	70(55)		AV 327	P1174001	*, NO
SK -68 75	B1 I	1	78		AV 327	A0490501-2	NO
SK -68 111	BN1 Ia	15	72		AV 327	B1280501	HD 269668, NO
SK -68 129	B1 I	5	96		AV 327	B0860501	NO
SK -68 135	ON9.7 Ia+	16	68	70 ^b	AV 327	P1173901	HD 269896
SK -68 137	O3 III(f [*])	16	107		SK -66 100	E5114201	
SK -68 155	B0.5	11	96		SK -66 100	B0860701	NO
SK -68 171	B1 Ia	6	71		AV 327	A0490801	NO
SK -69 43	B0.5 Ia	6	102		AV 327	B1280601	HD 268809, NO
SK -69 50	O7 If	7	178		AV 327	E5112001	
SK -69 52	B2 Ia	6	105		AV 327	P1174301	NO
SK -69 59	B0 Ia	11	111		AV 327	P1031103	
SK -69 94	A0e/LBV		127		AV 327	Z9050201	*,S Dor = HD 35343, NO
SK -69 104	O6 Ib(f)	3	117	97 ^b	AV 327	P1172401	HD 269357
SK -69 124	O9 Ib	3	96		AV 327	P1173601-2	
SK -69 223	WC4(+OB)	17	84		AV 327	P2150201-2	*HD 38029, Brey 67, NO
SK -69 237	B1 Ia	15	86		AV 327	B1280701	NO
SK -69 279	O9 f	2	84		AV 327	B0860801	
SK -70 13	O9 V	7	84		AV 327	D0981001	
SK -70 32	O9.5 II	18	97		AV 327	E5112501	
SK -70 60	O4-5 V:n	13	256		SK -66 100	P1172001	
SK -70 69	O5 V	3	98	131 ^a	AV 327	P1172101	
SK -70 78	B0.7 Ia	6	107		AV 327	B1280801	HD 269074
SK -70 79	B0 III	7	86		AV 327	B0900301	
SK -70 85	B0 I	1	63		AV 327	A0491301, A0491303	
SK -70 91	O2 III(f [*])+OB	3	99(78)		SK -66 100	P1172501	*, NO
SK -70 115	O7 Ib	4	164		AV 327	P1172601	
SK -70 120	B1 Ia	6	75		AV 327	A0491001-2	NO
SK -71 08	O9 II	2	75		AV 327	A0491401-2	
SK -71 19	O7 V	4	242		AV 327	E5113001	
SK -71 41	O8.5 I	7	53		AV 327	D0980501	
SK -71 45	O4-5 III(f)	3	117	125 ^b	SK -66 100	P1031501-4	HD 269676
SK -71 46	O4 If	7	79		SK -66 100	D0980601	
SK -71 50	O6.5 III	2	296		AV 327	A0491201	
BI 12	O6 III	4	116		AV 327	E5111802	
BI 13	O6.5 V	2	118		SK -66 100	E5111901	
BI 130	O8.5 V((f))	7	95		AV 327	E5112902	
BI 170	O9.5 Ib	3	84		AV 327	P1173701	
BI 173	O8 II:	3	116		SK -66 100	P1173201-2	*, NO
BI 208	O7 V	2	196		AV 327	P1172702-5	
BI 237	O2 V((f [*]))	10	83	126 ^a	SK -66 100	E5114001	
BI 253	O2 V((f [*]))	10	155	191 ^a	SK -66 100	C0020601-2	

Table 3—Continued

Star	Spectral Classification	Ref.	$\langle V \sin i \rangle$		Template Star	FUSE data sets	Notes
			This paper (km s ⁻¹)	Other (km s ⁻¹)			
BI 272	O7 III	19	212		AV 327	P1172901-2	
HV 2241	O7 III + B0 III	20	71		AV 327	F9270603	*, NO
LH47-338	O7 V((f))	5	99		AV 327	P2320101	N44C Star 2
LMC X-4	O8 III	21	322		AV 327	A0440102	*, NO
LMC2-703	O9.5 V	7	95		AV 327	D0981401	D301-1005
LMC2-755	O8 V	7	57		AV 327	D0981501	D301-NW8
PGMW 1486	O6.5 V	22	93		SK -66 100	D0300101	
PGMW 3053	O5.5 I-III(f)	22	110		SK -66 100	B0100101	
PGMW 3070	O6 V	22	72		AV 327	B0100201	
PGMW 3073	O6.5 V	22	71		AV 327	D0300201	
PGMW 3102	O7 V	22	68		AV 327	D0300302	
PGMW 3120	O5.5 V((f*))	22	111	95 ^b	SK -66 100	B0100301	
PGMW 3157	BC1 Ia	22	88		AV 327	B0100401	NO
PGMW 3168	O7 II(f)	22	78	96 ^a	SK -66 100	B0100501	
PGMW 3204	O6-7 V	22	78	130 ^a	SK -66 100	D0300402	
PGMW 3209	O3 III(f*)+OB	22	166		AV 327	B0100601	*, NO
PGMW 3223	O8.5 IV	22	147		SK -66 100	B0100701	
PGMW 3264	O3-6 V	22	56		SK -66 100	B0100801	

Note. — Spectral Classifications from (1) Jaxon et al. (2001), (2) Conti et al. (1986), (3) Walborn et al. (2002), (4) Smith Neubig & Bruhweiler (1999), (5) Massey et al. (2000), (6) Fitzpatrick (1988), (7) Massey et al. (1995), (8) Gummersbach et al. (1995), (9) Koenigsberger et al. (2003), (10) Massey et al. (2005), (11) Rousseau et al. (1978), (12) Fehrenbach & Duftot (1982), (13) Robert et al. (2003), (14) Bohannan & Walborn (1989), (15) Fitzpatrick (1991), (16) Walborn (1977), (17) Bartzakos et al. (2001), (18) Massey (2002), (19) Plante (1998), (20) Ostrov et al. (2001), (21) Negueruela & Coe (2002), and (22) Parker et al. (1992). $V \sin i$ values from (a) Mokiem et al. (2007) and (b) Penny et al. (2004). *Additional notes on individual stars are presented in the Appendix.

Table 4. SMC Stars with Previous $V \sin i$ Values

Star	Spectral Classification	$\langle V \sin i \rangle$ (km s ⁻¹)	Reference
346-010	O7 III _n ((f))	313	M06
346-012	B1 Ib	29	M06
346-018	O9.5 III _e	138	M06
346-022	O9 V	55	M06
346-025	O9 V	138	M06
346-031	O8 Vz	18	M06
346-033	O8 V	188	M06
346-046	O7 V _n	340	M06
346-050	O8 V _n	357	M06
346-051	O7 Vz	18	M06
346-066	O9.5 V	129	M06
346-077	O9 V	177	M06
346-090	O9.5 V	188	M06
346-093	B0 V	187	M06
346-097	O9 V	22	M06
346-107	O9.5 V	55	M06
346-112	O9.5 V	143	M06
330-013	O8.5 III((f))	73	M06
330-052	O8.5 V _n	291	M06
NGC346-MPG368	O4-5 V((f))	55	P04
NGC346-MPG113	OC6 Vz	<40	P04
AV 243	O6 V	62	P04
NGC346-MPG487	O6.5 V	65	P04
AV 220	O6.5f?p	<40	P04
NGC346-MPG682	O8 V	71	P04
NGC346-MPG12	O9.5-B0 V	67	P04
AV 170	O9.7 III	54	P04

Note. — M06 = Mokiem et al. (2006) and P04 = Penny et al. (2004)

Table 5. LMC Stars with Previous $V \sin i$ Values

Star	Spectral Classification	$\langle V \sin i \rangle$ (km s ⁻¹)	Reference
N11-004	OC9.7 Ib	81	M07
N11-008	B0.7 Ia	83	M07
N11-026	O2 III(f*)	109	M07
N11-029	O9.7 Ib	77	M07
N11-031	ON2 III(f*)	116	M07
N11-033	B0 III _n	256	M07
N11-036	B0.5 Ib	54	M07
N11-038	O5 II(f+)	145	M07
N11-042	B0 III	42	M07
N11-045	O9 III	105	M07
N11-051	O5 V _n ((f))	333	M07
N11-058	O5.5 V((f))	85	M07
N11-060	O3 V((f*))	106	M07
N11-061	O9 V	87	M07
N11-065	O6.5 V((f))	83	M07
N11-066	O7 V((f))	71	M07
N11-068	O7 V((f))	54	M07
N11-072	B0.2 III	14	M07
N11-087	O9.5 V _n	276	M07
N11-123	O9.5 V	110	M07
HD 269810	O2 III(f*)	173	P04
SK -69 212	O5 III(f)	210	P04
SK -67 51	O6.5 III	105	P04
CD -68 264	O8 V	139	P04
LH58-52A	O8 II	110	P04
LH58-19A	O9 II	178	P04

Note. — M07 = Mokiem et al. (2007) and P04 = Penny et al. (2004)

Table 6. Kolmogorov-Smirnov Statistics

Sample 1	n_1 stars	$\langle V \sin i \rangle$ (km s ⁻¹)	Sample 2	n_2 stars	$\langle V \sin i \rangle$ (km s ⁻¹)	D	p (%)
Unevolved Vs. Evolved Within Each Environment							
Galactic unevolved	79	129.8	Galactic evolved	56	109.5	0.296	0.5
LMC unevolved	36	132.0	LMC evolved	42	118.6	0.151	74
SMC unevolved	32	116.2	SMC evolved	19	101.8	0.289	23
Unevolved Samples							
LMC unevolved	36	132.0	Galactic unevolved	79	129.8	0.180	37
SMC unevolved	32	116.2	Galactic unevolved	79	129.8	0.172	47
SMC unevolved	32	116.2	LMC unevolved	36	132.0	0.295	8
Evolved Samples							
LMC evolved	42	118.6	Galactic evolved	56	109.5	0.321	1
SMC evolved	19	101.8	Galactic evolved	56	109.5	0.297	13
SMC evolved	19	101.8	LMC evolved	42	118.6	0.137	95

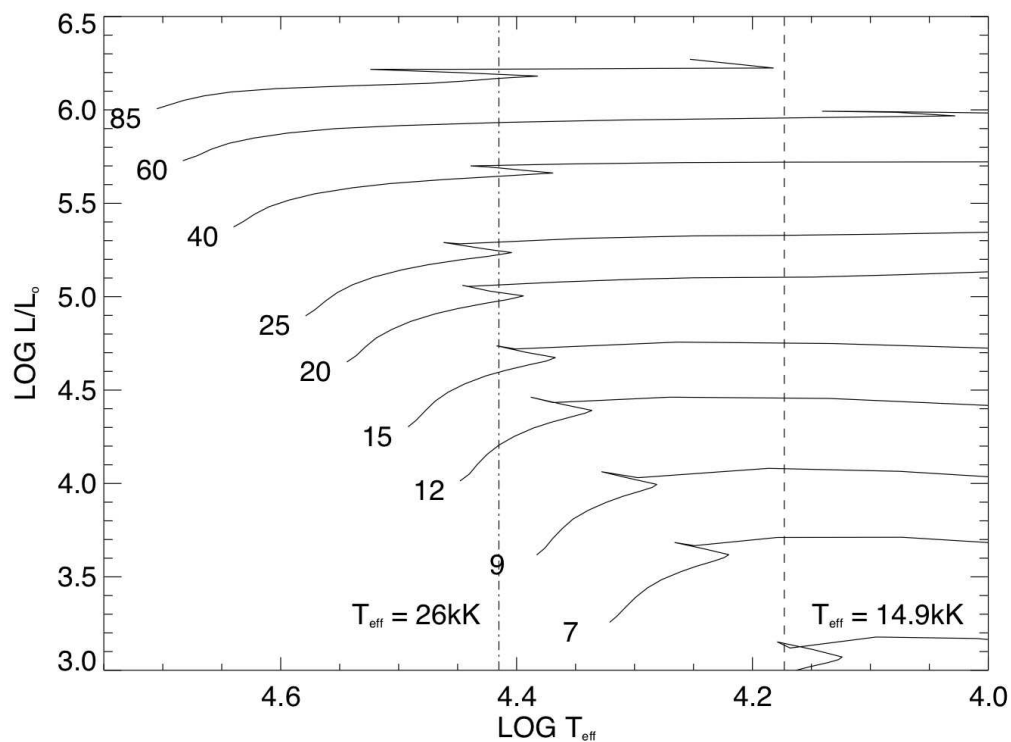


Fig. 1.— Evolutionary tracks from Schaller et al. (1992) with an overlain lines at $T_{\text{eff}} = 26000\text{K}$ and $T_{\text{eff}} = 14900\text{K}$. The first corresponds to spectral class O9.7 I by Crowther et al. (2002), presumably the lower limit of effective temperatures to be assigned to O spectral type stars. All stars to the right of this line will be typed as B types or cooler. The second overlaid line corresponds to the temperature for spectral classification B3 I (Bohm-Vitense 1981). Stars with this temperature may have progenitors with initial masses as low as $7M_{\odot}$.

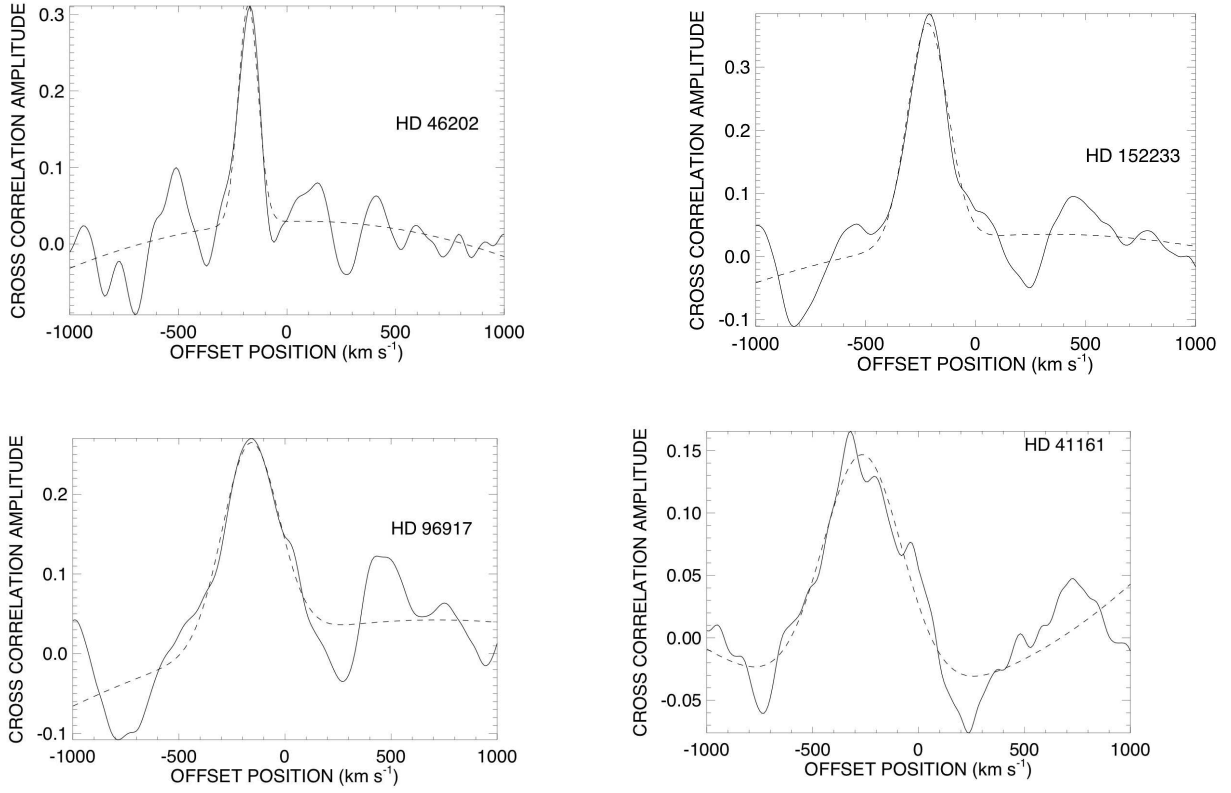


Fig. 2.— The cross-correlation functions and Gaussian fits for the Galactic stars (a) HD 46202 (O9 V; $V \sin i = 37 \text{ km s}^{-1}$), b) HD 152233 (O6 III:(f)p; $V \sin i = 104 \text{ km s}^{-1}$), (c) HD 96917 (O8.5 Ib(f); $V \sin i = 176 \text{ km s}^{-1}$), (d) HD 41161 (O8 Vn; $V \sin i = 304 \text{ km s}^{-1}$). The bumpy nature of the ccf for HD 41161 may be indicative of non-radial pulsations.

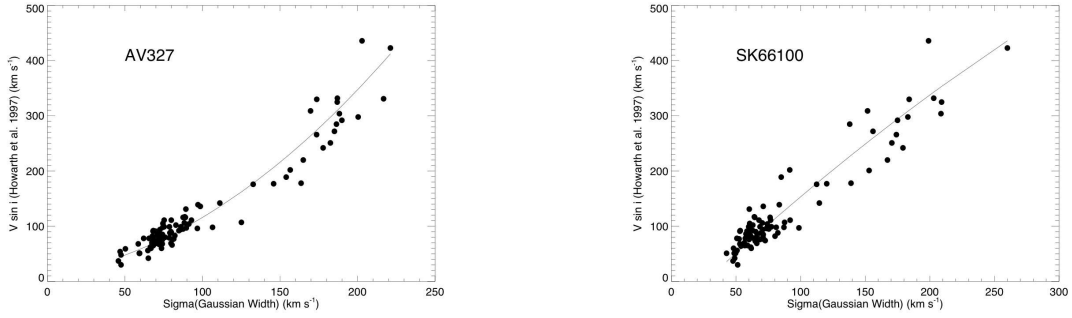


Fig. 3.— The projected rotational velocities of Penny (1996) or Howarth et al. (1997) from IUE spectra vs. the Gaussian width of the CCF’s from the template (a) AV 327 (O9.5 II-Ibw) and (b) SK -66 100 (O6 II(f)).

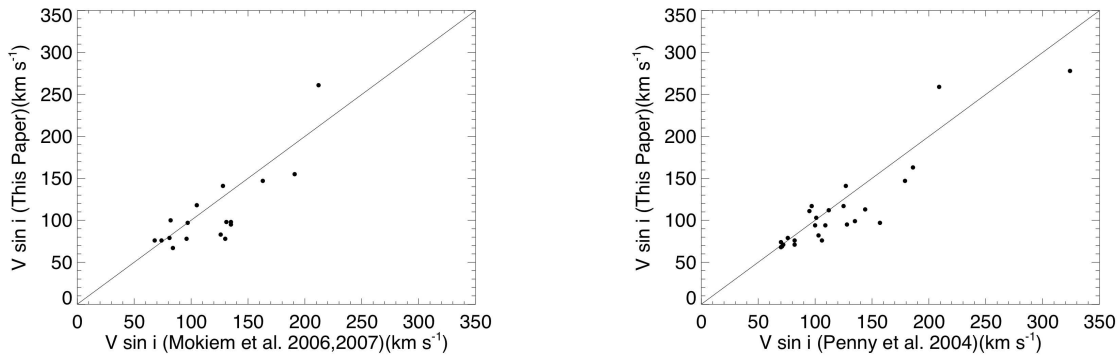


Fig. 4.— Projected rotational velocities from Tables 2 and 3 versus (a) Mokiem et al. (2006, 2007) and (b) Penny et al. (2004) for those targets in common.

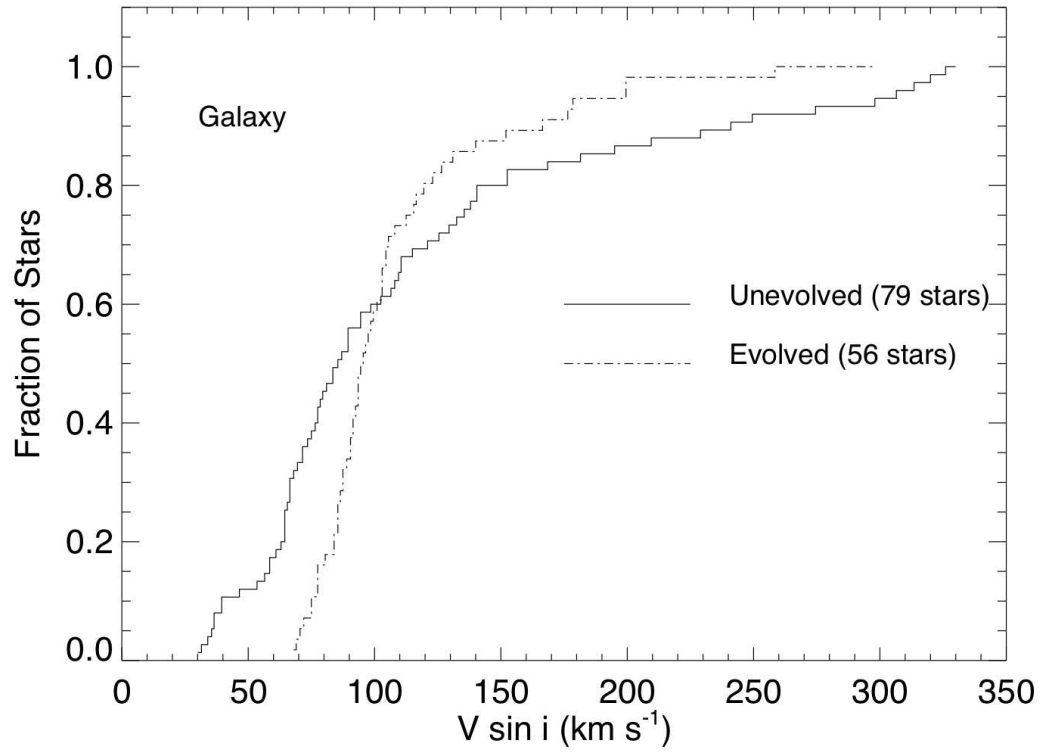


Fig. 5.— Cumulative distribution functions of $V \sin i$ values for unevolved and evolved stars in the Milky Way.

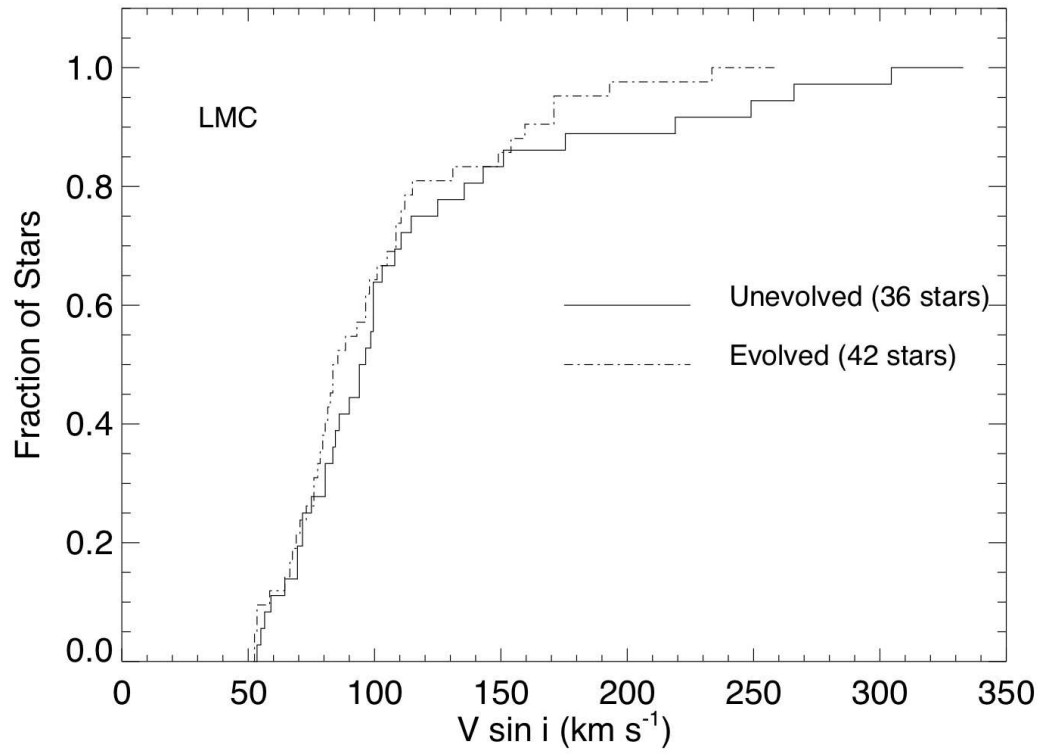


Fig. 6.— Cumulative distribution functions of $V \sin i$ values for unevolved and evolved stars in the LMC.

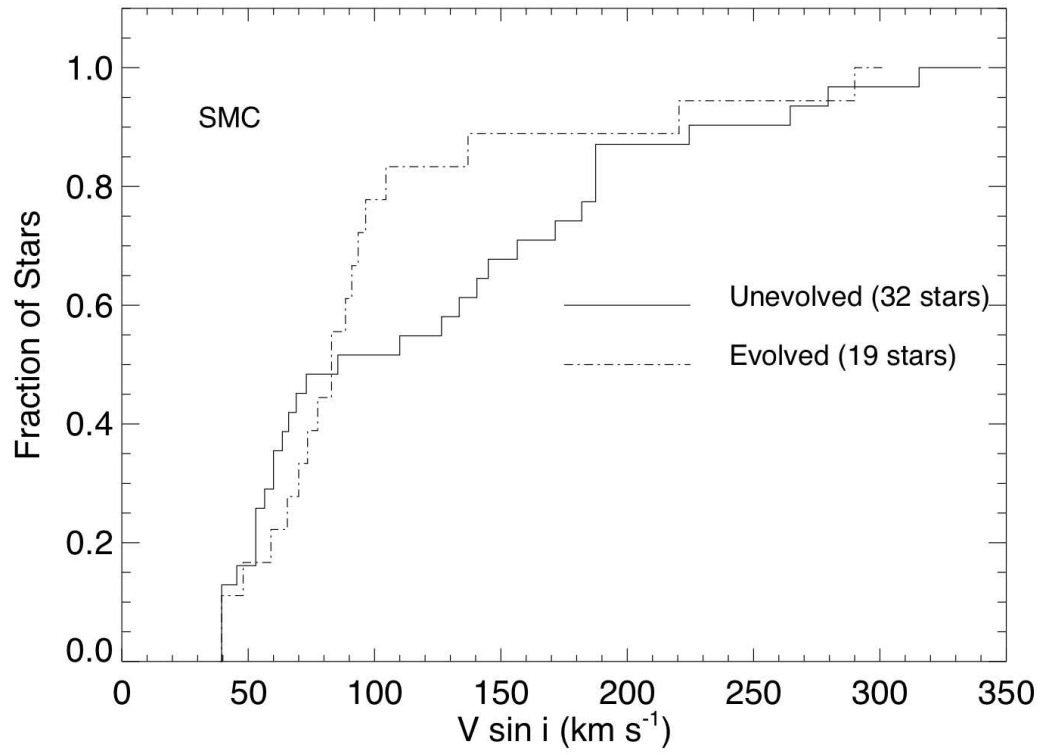


Fig. 7.— Cumulative distribution functions of $V \sin i$ values for unevolved and evolved stars in the SMC.

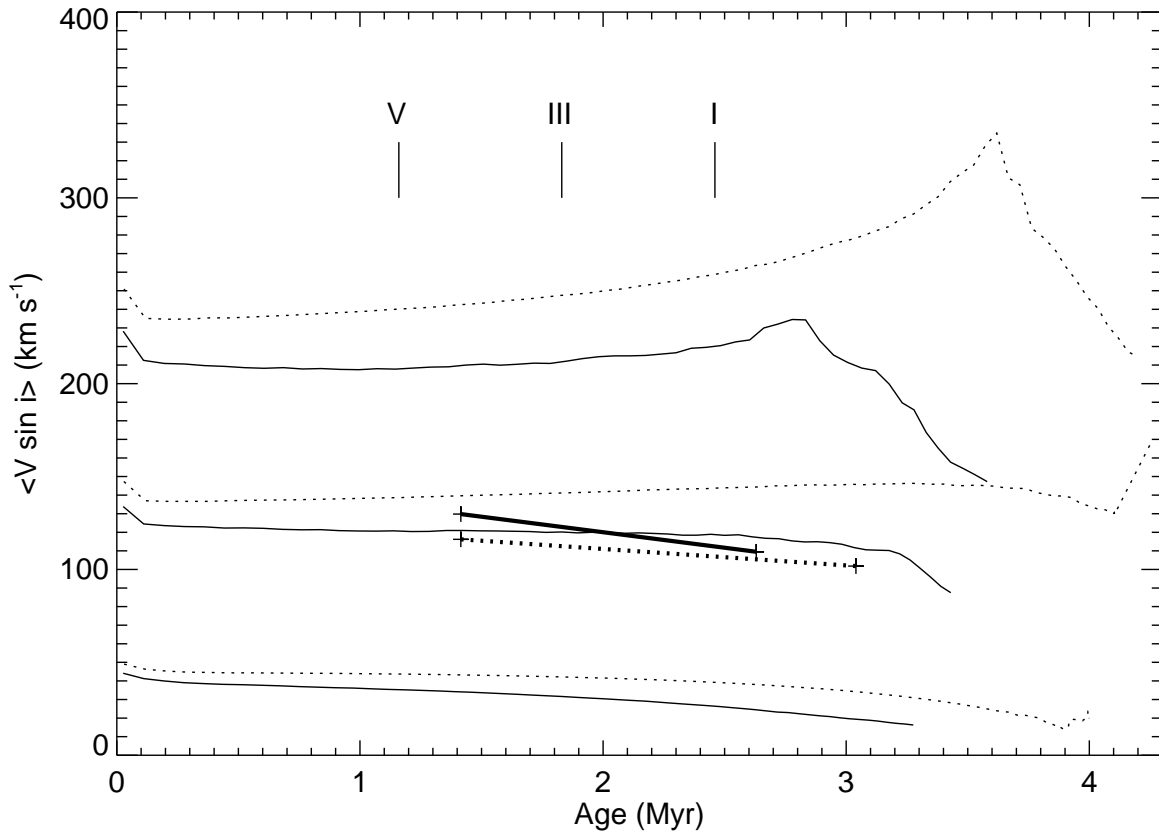


Fig. 8.— Predicted changes in mean $V \sin i$ with age for $60M_{\odot}$ models from ?. The thin solid lines show the variations for Galactic abundance stars with initial ratios of equatorial to critical angular velocity of 0.5, 0.3, and 0.1 (*from top to bottom*), while the thin dotted lines show the same for SMC abundance stars. All these tracks are terminated at an age where the star cools enough to become a B-supergiant. The thick solid and dotted lines that connect plus signs show the observed change in average $V \sin i$ between the unevolved and evolved groups for the Galactic and SMC samples, respectively.

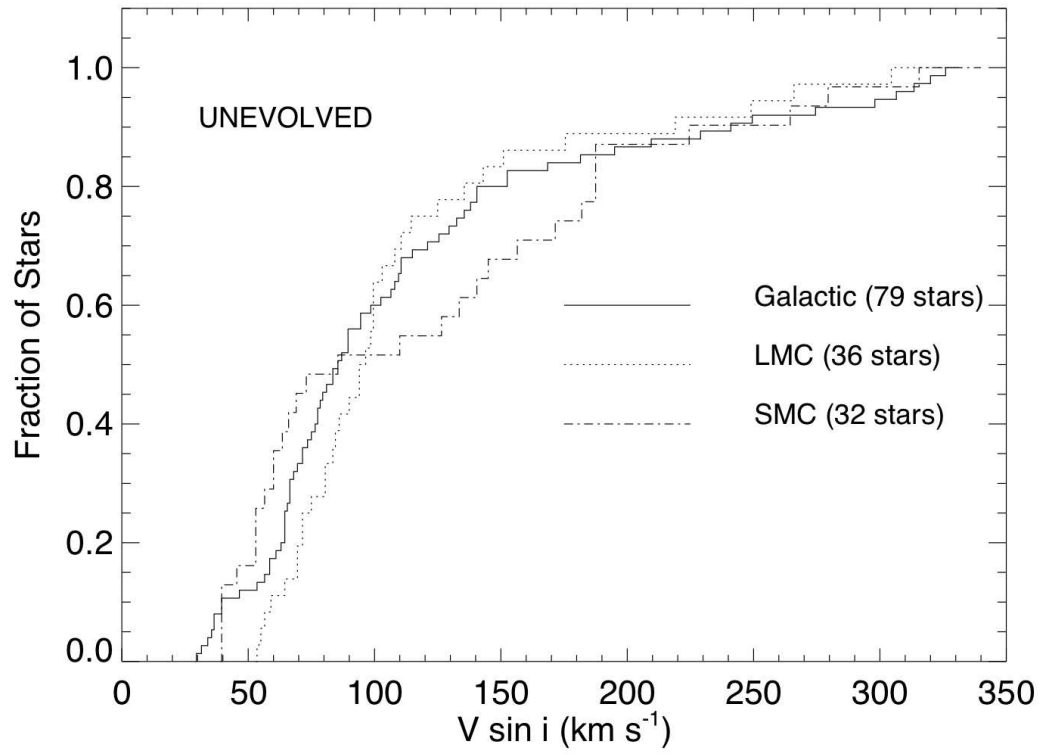


Fig. 9.— Cumulative distribution functions of $V \sin i$ values for unevolved (luminosity classes IV - V) stars in the SMC, LMC and Galaxy.

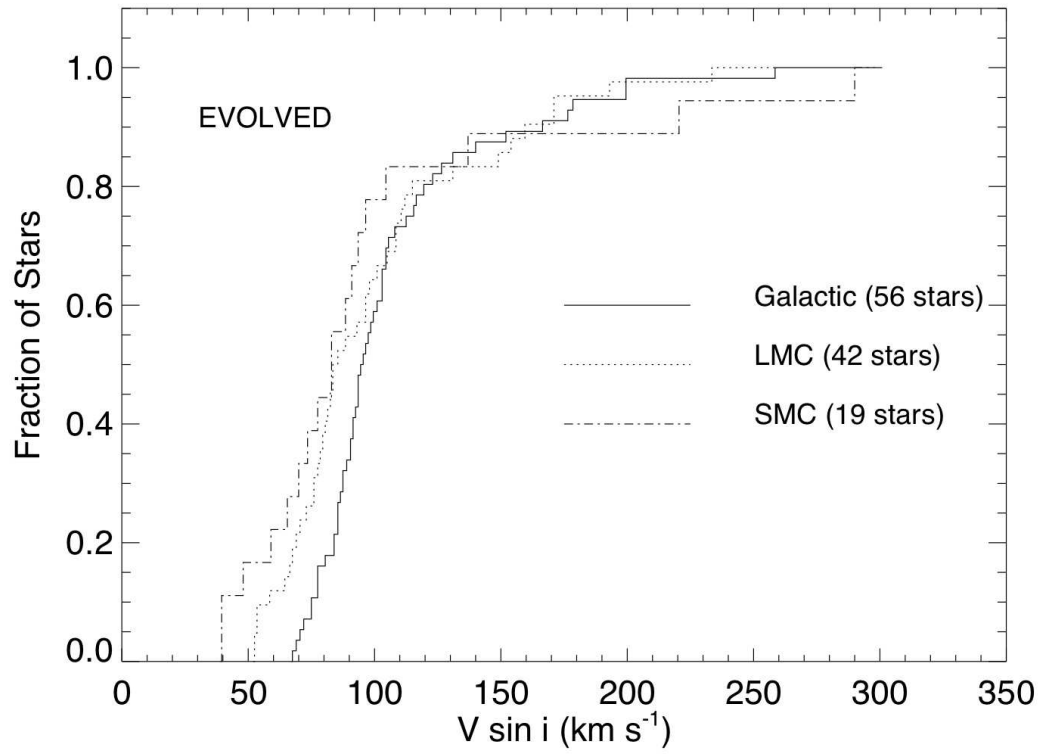


Fig. 10.— Same as Figure 9 but for evolved (luminosity classes I-II) stars in the same three environments.